

Journal of Biomedical Optics

SPIEDigitalLibrary.org/jbo

High-density diffuse optical tomography of term infant visual cortex in the nursery

Steve M. Liao
Silvina L. Ferradal
Brian R. White
Nicholas Gregg
Terrie E. Inder
Joseph P. Culver

High-density diffuse optical tomography of term infant visual cortex in the nursery

Steve M. Liao,^{a*} Silvina L. Ferradal,^{b,c*} Brian R. White,^{c,d} Nicholas Gregg,^e Terrie E. Inder,^a and Joseph P. Culver^{b,c,d}

^aWashington University School of Medicine, Department of Pediatrics, 660 S. Euclid Ave, St. Louis, Missouri 63110

^bWashington University, Department of Biomedical Engineering, Whitaker Hall, Campus Box 1097, One Brookings Drive, St. Louis, Missouri 63130

^cWashington University School of Medicine, Department of Radiology, 660 S. Euclid Ave, St. Louis, Missouri 63110

^dWashington University, Department of Physics, Campus Box 1105, One Brookings Drive, St. Louis, Missouri 63130

^eUniversity of Pittsburgh School of Medicine, M240 Scaife Hall, 3550 Terrace Street, Pittsburgh, Pennsylvania 15261

Abstract. Advancements in antenatal and neonatal medicine over the last few decades have led to significant improvement in the survival rates of sick newborn infants. However, this improvement in survival has not been matched by a reduction in neurodevelopmental morbidities with increasing recognition of the diverse cognitive and behavioral challenges that preterm infants face in childhood. Conventional neuroimaging modalities, such as cranial ultrasound and magnetic resonance imaging, provide an important definition of neuroanatomy with recognition of brain injury. However, they fail to define the functional integrity of the immature brain, particularly during this critical developmental period. Diffuse optical tomography methods have established success in imaging adult brain function; however, few studies exist to demonstrate their feasibility in the neonatal population. We demonstrate the feasibility of using recently developed high-density diffuse optical tomography (HD-DOT) to map functional activation of the visual cortex in healthy term-born infants. The functional images show high contrast-to-noise ratio obtained in seven neonates. These results illustrate the potential for HD-DOT and provide a foundation for investigations of brain function in more vulnerable newborns, such as preterm infants. © 2012 Society of Photo-Optical Instrumentation Engineers (SPIE). [DOI: 10.1117/1.JBO.17.8.081414]

Keywords: diffuse optical imaging; near infrared spectroscopy; visual response; infants; brain.

Paper 11794SS received Dec. 28, 2011; revised manuscript received Jun. 5, 2012; accepted for publication Jun. 8, 2012; published online Jul. 9, 2012.

1 Introduction

Although increasing numbers of infants now survive preterm birth, the risk of long-term disability in this population has remained constant over the last two decades.¹ To date, structural neuroimaging studies have demonstrated only modest correlation with neurodevelopmental outcomes, and the major pathophysiological mechanisms leading to adverse outcomes are not yet fully understood. Characterization of the maturation of functional neural networks may provide new insights that better define the functional “lesions” associated with prematurity that lead to neurodevelopmental impairments. Recent investigations with functional connectivity magnetic resonance imaging (fcMRI) have established the patterns of functional network development in preterm infants and demonstrated marked differences in functional connections between preterm infants at term equivalent postmenstrual age and term control infants.^{2,3} However, there are challenges in acquiring fcMRI in premature infants due to risks associated with transportation to a remote scanner. Furthermore, frequent scanning is required to capture the rapid evolution of brain development. Thus in order to better understand the nature and timing of alterations in cerebral function, bedside methods for evaluating brain function are needed.

Noninvasive optical neuroimaging methods offer bedside availability, and new advances with high-density diffuse optical tomography (HD-DOT) now provide improved image quality.⁴⁻⁶

Recently, functional connectivity methods have been extended to DOT (fcDOT) in adults.⁷ Parallel pilot studies have recently demonstrated the feasibility of imaging infants with fcDOT.⁸ While resting state imaging methods have advantages in infants that can generally perform few tasks, stimulus-related imaging studies are needed for validation and interpretation of resting state analyses.⁹ Activation studies are used routinely in conjunction with resting state functional connectivity evaluations to establish functional landmarks that locate or affirm seed positions used in correlation analysis.⁹ Moreover, they can be used to query the sensory input portions of the central nervous system that are bypassed in cortical-cortical functional connectivity analysis.¹⁰ In adults, HD-DOT activation imaging has been established using sensorimotor^{11,12} and visual stimulus paradigms.⁶ In infants, sparse near-infrared spectroscopy (NIRS) studies have shown that the visual evoked response can be recorded in sleeping neonates¹³ and awake infants.^{14,15} Although promising, the sparse NIRS approaches suffer from methodological issues related to the ability of effectively distinguishing evoked-responses from confounding hemodynamic signals localized to superficial tissue layers.^{16,17} Alternatively, HD-DOT can sample tissue at different depths within the field of view of the imaging array, allowing for superficial signal regression procedures that help to minimize the influence of physiological noise.^{6,18,19} In this paper, we use an extended field of view system that samples the majority of the primary visual cortex and establish the capability of HD-DOT imaging arrays to image the

*These authors contributed equally to this work.

Address all correspondence to: Joseph P. Culver, Washington University School of Medicine, Department of Radiology, 4525 Scott Avenue, Room 1137, St. Louis, Missouri 63110. Tel: 314-747-1341; E-mail: Culverj@mir.wustl.edu

hemodynamic response in the occipital cortex to visual stimulus in term-born infants at the bedside.

2 Methods

2.1 Subjects

We recruited 11 healthy term-born infants (>37 weeks completed gestational age) in the first two days of life from our newborn nursery at Barnes-Jewish Hospital. The study was approved by the Human Research Protection Office of the Washington University School of Medicine, and informed consent was obtained from the parent(s) of each participating infant before scanning. The characteristics of each subject are summarized in Table 1. A physician examined each infant and reviewed the medical chart prior to the study to ensure overall health. All infants were observed to be resting or sleeping comfortably in their bassinets during the entire scanning sessions.

2.2 Instrumentation

We previously developed a high-density, multi-channel, continuous wave, diffuse optical imaging system using light emitting diode (LED) sources and avalanche photodiode detectors. Each source position consisted of two near-infrared wavelengths (750 and 850 nm) of light emitting diodes (LEDs). The system operates in continuous wave mode with a frame rate of 10.78 Hz. This simple and modular instrumentation provides scalability to construct a portable system with a capacity of 18 source positions and 16 detector positions, providing a total of 168 measurements (48 first nearest-neighbor, 58 second nearest neighbor, 14 third nearest neighbor, 36 fourth nearest neighbor,

and 12 fifth nearest neighbor pairs). Flexible optical fibers with a diameter of 2.5 mm were used to carry light signals. The imaging pad consists of a high-density source-detector fiber array held in a soft neoprene/silicone cap strapped by elastic neoprene/Velcro material to the back of the infant's head (Fig. 1).

2.3 Protocol

The center of the imaging pad was positioned slightly above theinion, over surface landmarks for the visual cortex (Fig. 1). All scans were taken within 2 h after feeding in an isolated and dimly lit room in the well infant nursery at Barnes Jewish Hospital, St Louis. The timing of the scan was chosen to maximize infant cooperation. Visual stimulation was provided by a 19-inch liquid-crystal-display monitor at 20 cm away from the infant's face. The visual stimulus consisted of two counter-phase checkerboard patterns containing 10 rows and 10 columns of squares (total luminance of 50%) and an alternating 0% flat luminance pattern. A full one-second stimulus included a sequence of checkerboard, flat, counter-phase checkerboard, and flat frames. Note that the visual stimulus used was designed to work in a broader range of situations than encountered in the current study. Changes in the net luminance between the dark screen and the checkerboard patterns stimulate visual responses in subjects with closed eyes, while the reverse checkerboard patterns provide strong visual responses in awake subjects. In this particular study, since the infant's eyes were closed, the stimulus was due to the change in luminance at 4 Hz. Each block of visual stimulus was defined by 10 s of stimulus followed by 20 s of black screen. The stimulus block was repeated for approximately 15 min, depending on the infant's cooperativeness. Although the infants' eyes remained closed throughout the

Table 1 Clinical characteristics of each subject.

ID	Gender	Race	Gestational age at birth (weeks)	Age at scan (days)	Mode of delivery
1	F	AA	37 4/7	1	Vag.
2*	F	AA	38 3/7	2	Vag.
3*	M	AA	39 0/7	2	C/S
4	F	AA	38 6/7	1	Vag.
5	F	C	39 0/7	2	C/S
6*	F	AA	40 0/7	2	Vag.
7	M	AA	38 6/7	1	Vag.
8*	F	Hisp.	38 2/7	2	Vag.
9	F	AA	40 3/7	1	C/S
10	M	AA	40 3/7	2	Vag.
11	M	C	39 0/7	2	C/S
Mean	—	—	39 0/7	1.7	—

^a(M = male; F = female; AA = African American, C = Caucasian, Hisp. = Hispanic, C/S = Cesarean-section, Vag. = Vaginal delivery).
*Data from these infants were excluded from further analysis due to excessive noise level likely from motion artifact.

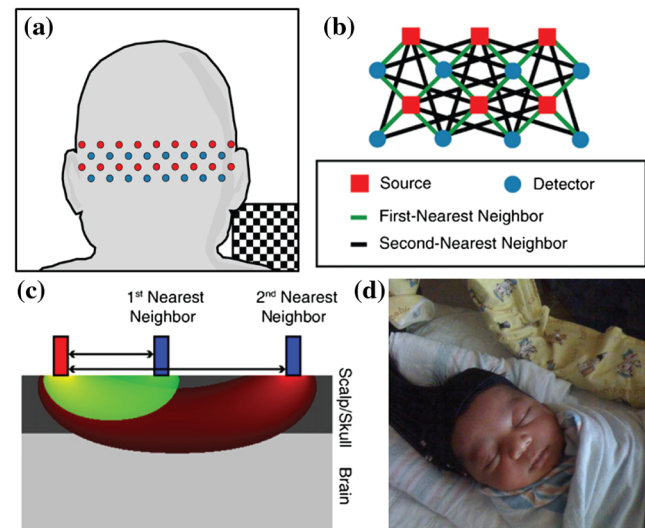


Fig. 1 Our high-density diffuse optical tomography system. (a) Schematic diagram showing the placement of the imaging array over the occipital cortex of an infant. (b) Schematic diagram showing the arrangement of first- and second-nearest neighbors within a subset of this array. (c) A cross-sectional view of source-detector relationship with the first-nearest neighbor source-detector pair sampling mostly superficial signal coming from the scalp/skull and the second-nearest neighbor source-detector pair sampling a mixture of signals (both from the superficial layer and the brain activity). Signals from the superficial layer can then be regressed out of the deeper mixed signals, therefore improving the system's brain specificity. (d) A picture showing a term-born healthy infant comfortably wearing our imaging cap over the occipital cortex during a scanning session.

scans, previous studies using similar visual stimulation patterns have demonstrated the feasibility of measuring visual evoked responses in sleeping newborn infants.^{15,20,21}

2.4 Data Analysis

A possible way to evaluate the performance of our imaging method is by comparisons with standard sparse NIRS analysis. Therefore, two reconstruction approaches were considered in the present study: a) single source-detector (SD) pair NIRS analysis without superficial signal regression (sparse NIRS); and b) tomographic reconstructions with superficial signal regression (high-density DOT).

Several pre-processing steps are common to both reconstruction approaches. First, the detector light levels were decoded to SD pair data (considered to be a single channel). We took the logarithm of the ratio of each channel's level to its mean, which yielded time traces of differential light intensity for each wavelength. The log-ratio data was band-pass filtered (0.02 to 0.5 Hz) to remove long-term drift and pulse artifacts. The filtered SD pair measurements were then divided into stimulus blocks. Stimulus blocks that exhibited high temporal variance (>7.5%) were considered to be corrupt (likely due to motion artifacts) and were excluded from further analysis.

For sparse NIRS analysis, the log-ratio data was converted to absorption changes using the modified Beer-Lambert law. For the differential path length factor, we used values reported in Ref. 22) of 5.11 and 4.67 for 750 and 850 nm, respectively. Although the reported values were measured at 744 and 832 nm, this level of approximation is appropriate because the hemoglobin spectrum does not show high variability in these regions (744 to 750 nm and 832 to 850 nm). Furthermore, since the full-width half maximum bandwidth of the LED spectra is 30 nm, any spectral change within this range will be effectively smoothed. Concentration changes of oxy- (ΔHbO_2), deoxy- (ΔHbR), and total hemoglobin (ΔHbT) were computed using the extinction coefficients of both hemoglobin species.²³

Our high-density array allows us to obtain measurements at multiple distances (Fig. 1). Thus for the DOT analysis, we focus on the first- and second-nearest neighbor pairs with a SD pair distance of 1 and 2.2 cm, respectively. First-nearest neighbor measurements are primarily sampling superficial hemodynamic signals from the scalp and skull, while second-nearest neighbor measurements are also sensitive to brain hemodynamics. In order to minimize systemic and superficial contamination, we regressed out an average of the first-nearest neighbor measurements from all of the individual measurements.^{16,17,24}

For the DOT reconstructions, a finite-element forward model derived from a two-layer hemispherical model was used to generate a sensitivity matrix.²⁵ The mesh contained 22,731 nodes, and after light modeling the sensitivity matrix was interpolated to a 2 mm square voxel-grid. Optical properties (absorption coefficient: μ_a and reduced scattering coefficient: μ_s') for the two-layer hemispherical model were obtained from Ref. 26. We used $\mu_a = 0.15 \text{ cm}^{-1}$, $\mu_s' = 8.4 \text{ cm}^{-1}$ at 750 nm and $\mu_a = 0.17 \text{ cm}^{-1}$, $\mu_s' = 7.4 \text{ cm}^{-1}$ at 850 nm for the outer scalp/skull layer. Similarly for the inner brain layer, we used $\mu_a = 0.19 \text{ cm}^{-1}$, $\mu_s' = 12 \text{ cm}^{-1}$ at 750 nm, and $\mu_a = 0.19 \text{ cm}^{-1}$, $\mu_s' = 11 \text{ cm}^{-1}$ at 850 nm. While these values were obtained from adults, studies comparing optical properties in adults and infants have generally shown similar optical properties in both groups,²⁷ and most NIRS/DOT studies of infants use adult values for relevant head averaged optical constants.^{28,29}

The sensitivity matrix was inverted once per subject per run in order to account for first- and second-nearest neighbor channels corresponding to the stimulus blocks that passed the earlier noise threshold (i.e., blocks that exhibited a temporal variance <7.5%). Using the inverted sensitivity matrix, log-ratio data was converted into volumetric reconstructions of absorption changes for both 750 and 850 nm. Tomographic maps of ΔHbO_2 and ΔHbR were then computed using the same extinction coefficients.

As we were interested in hemodynamic responses within the cortex, we selected a cortical shell (1 cm thickness) from within our three-dimensional (3-D) data set and averaged across the thickness of the shell. All HD-DOT images displayed are posterior coronal projections of this cortical shell (i.e., we have averaged along the anterior-posterior axis), resulting in a point-of-view as if looking at the head from behind with the skin and skull removed. The field of view is 13 cm in width and 4 cm in height; each pixel is 2 by 2 mm. DOT simultaneously creates images of ΔHbO_2 , ΔHbR , and ΔHbT . For simplicity, all images shown here are ΔHbO_2 . The images in the other contrasts are qualitatively similar (i.e., increasing and decreasing trends in ΔHbT and ΔHbR , respectively).

To perform a direct comparison between the NIRS and DOT approaches, we compared the temporal traces. For DOT, a region of interest (ROI) was defined based on the 1 cm³ volume with the maximum response (between 10 and 14 s post stimulus) in the ΔHbO_2 maps. Temporal traces extracted from this ROI were averaged for ΔHbO_2 , ΔHbR , and ΔHbT concentration changes. For sparse NIRS, we only considered second-nearest neighbor measurements, which are sensitive to the brain. Thus the single second-nearest neighbor measurement with the greatest sensitivity to the peak DOT response was selected for comparison with the averaged temporal traces obtained from the DOT maps.

For statistical analysis, hemoglobin time traces were down sampled to 0.2 Hz (5 s intervals). The changes at the peak were compared to the 5 s baseline around stimulus onset using a Student's *t*-test. The *t*-statistic was converted to a *p*-value using both tails of the distribution (i.e., no directionality to the response was assumed). Significance was inferred for all *p*-values with $\alpha < 0.05$.

To have an objective measure of signal quality, we also calculated contrast-to-noise ratios (CNR) for tomographic data and sparse NIRS data for each subject. CNR was calculated as the ratio of the peaked signal intensity (averaged over multiple stimulus presentations) and the baseline noise (given by the standard deviation in the pre-stimulus baseline).

3 Results

We were able to obtain diffuse optical tomography images of the visual cortex in response to the flashing visual stimulus in seven out of the 11 infants recruited for this study. The data from four infants did not pass the predetermined noise threshold tests in our noise detection algorithm and were excluded from further processing (Table 2). A typical spatiotemporal hemodynamic response for ΔHbO_2 in a single infant is shown in Fig. 2(a). A bilateral increase in ΔHbO_2 concentration in response to the 10 s visual stimulus can be observed. The response peaked between 10 and 14 s and then slowly decayed towards the baseline. We observed the same general pattern in most of the infants as shown in Fig. 3. However, infants four and six showed asymmetrical activations of the visual cortices, and infants three and five showed prolonged activations.

Table 2 Contrast-to-noise ratios obtained for NIRS and DOT reconstruction for each subject.

ID	NIRS			DOT			Fold-improvement		
	ΔHbO_2	ΔHbR	ΔHbT	ΔHbO_2	ΔHbR	ΔHbT	ΔHbO_2	ΔHbR	ΔHbT
1	0.88	0.92	0.81	2.10	0.64	2.10			
2	*	*	*	*	*	*	*	*	*
3	*	*	*	*	*	*	*	*	*
4	1.80	0.18	1.60	5.70	0.96	6.40			
5	0.97	1.30	1.20	2.10	1.30	1.00			
6	*	*	*	*	*	*	*	*	*
7	2.20	3.10	1.20	4.70	1.00	4.30			
8	*	*	*	*	*	*	*	*	*
9	1.20	4.00	0.61	1.90	2.10	1.30			
10	3.10	3.30	1.80	3.10	3.60	1.20			
11	2.00	-1.10	2.00	2.00	0.70	1.70			
Mean	1.46	1.67	0.97	3.09	1.47	2.57	2.12	0.88	2.63

^aNIRS = near-infrared spectroscopy; DOT = diffuse optical tomography.

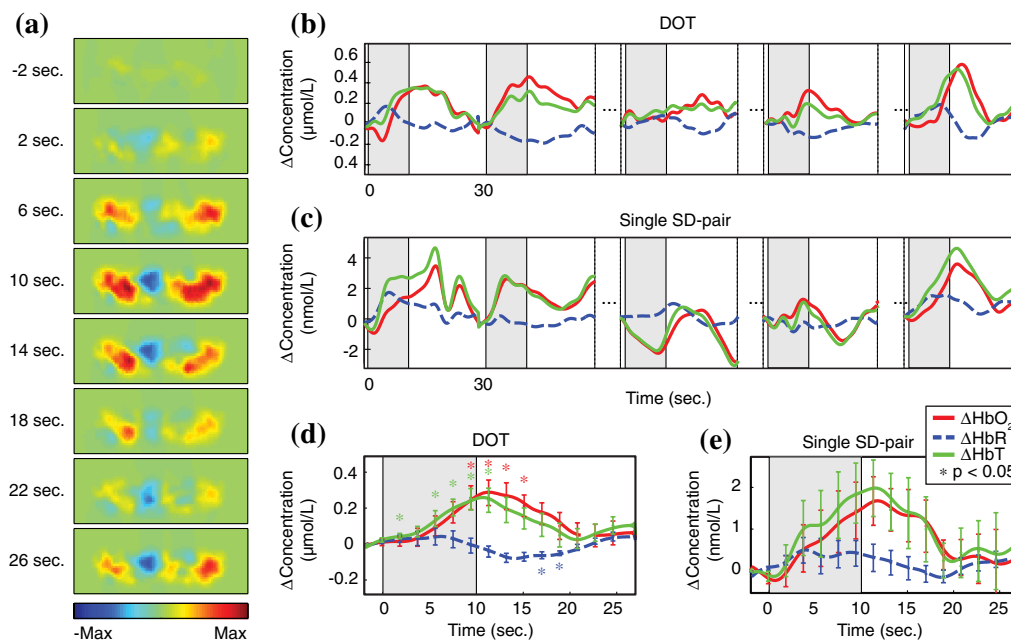


Fig. 2 DOT response in a healthy full-term infant. (a) Spatiotemporal hemodynamic response for ΔHbO_2 . Note the bilateral pattern in response to the 10-second visual stimulus. (b) to (c) Average temporal traces for the 1 cm^3 volume with the maximum response in the ΔHbO_2 maps versus single channel measurement over a span of five stimulus blocks. Note that some of the original blocks were removed due to noise thresholds. Dashed lines denote processed blocks that are not temporally adjacent. (d) to (e) Block average time trace of the peak 1 cm^3 ROI versus single channel measurement. Error bars mark standard deviation and asterisks indicate statistically significant deviation from baseline (two-tailed Student's *t*-test, $\alpha < 0.05$).

We also examined the temporal traces extracted from the maximal responses for both tomographic images and single source-detector pair (channel) NIRS measurements. Figure 2(b) displays the averaged temporal traces of the maximum 1 cm^3 ROI for the three hemodynamic contrasts and multiple blocks, while Fig. 2(c) displays the temporal traces associated to the

single channel with the greatest sensitivity to the peak voxel in the tomographic images. Similarly, block averaged temporal traces of the peak voxels and single channel measurements are shown in Fig. 2(d) and 2(e), respectively. It is worth to notice that the processed blocks are not necessarily temporally adjacent. Some of the original blocks were removed due to noise

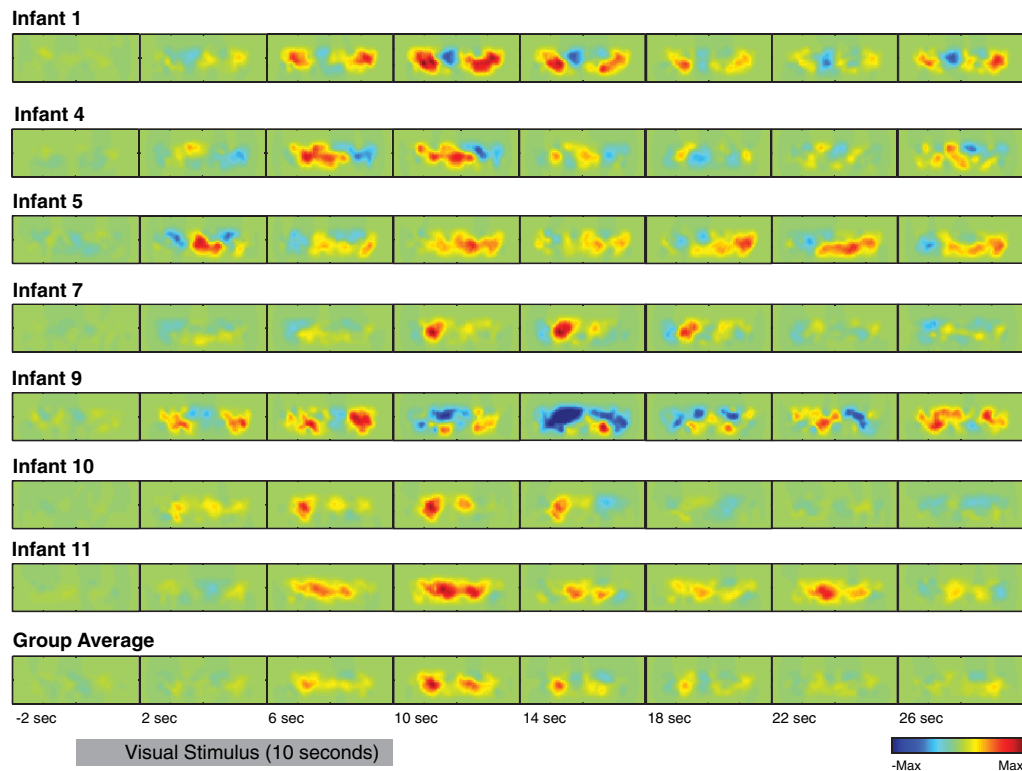


Fig. 3 DOT response in the visual cortex for a cohort of seven healthy, term-born infants. The imaging contrast is given by changes in oxy-hemoglobin concentration (ΔHbO_2). In general, we see a bilateral pattern of activation in response to the visual stimulus as confirmed by the group-averaged images.

thresholds. Therefore, the sharp changes that occur between some blocks do not reflect high-frequency noise, and the time courses average out predictably during the block averaging.

In addition, note that there is an almost two orders of magnitude difference between the traces obtained with the NIRS and DOT approaches. These differences can be explained as a partial volume effect that the NIRS method suffers due to its limited spatial resolution relative to the focality of the hemodynamic response. This effect has been observed and described in previous NIRS studies (please see Ref. 30 for a thorough analysis).

These results show the ability of the DOT reconstruction to reduce noise (error bars denote standard error for multiple blocks), improve statistical significance (asterisks mark significant deviation from baseline $p < 0.05$) and qualitatively improve the shape of the hemodynamic response. The improvement in DOT versus NIRS signal quality is also evident in terms of the contrast to noise ratio as shown in Table 2. For the tomographic imaging, the average CNR is 3.09, 1.47, and 2.57 for ΔHbO_2 , ΔHbR , and ΔHbT , respectively. For the single channel measurements, the corresponding CNR values are 1.46, 1.67, and 0.97. These results show a clear CNR increase of the DOT signals in comparison to the NIRS data for ΔHbO_2 and ΔHbT . However, this improvement is not evident in the case of ΔHbR , where CNR for NIRS and DOT are comparable.

4 Discussion

Our results show that high-density DOT can be successfully applied in neonates at the bedside of the well-baby nursery to image cerebral hemodynamic responses to stimulated brain activity within a short scanning time (15 min). Previously, we demonstrated the feasibility of using a high-density array

in infants with a restricted field of view (4 sources \times 10 detectors).²⁰ By extending the coverage of our imaging pad to 18 sources \times 16 detectors, we were able to obtain diffuse optical tomography images of the full occipital cortex in seven full-term infants.

Functional NIRS studies conducted in infants have typically interrogated primary sensory processes. In particular, visual^{13,31} and auditory³² processes have been monitored using sparse non-imaging arrays with SD-pair distances larger than 2.0 cm. A work by Taga et al.¹⁵ extended this approach by performing NIRS imaging of the visual cortex in awake infants and, more recently, Sato et al.³³ employed a whole-head optical topography technique to study hemodynamic responses in neonates exposed to speech sounds. A few recent studies have extended NIRS to higher-order functions.^{34,35} The majority of these studies used either solely time traces from single source-detector measurements or images made with topographic back-projection methods. The sparseness of the imaging arrays limits resolution, introduces uneven spatial sampling, and the data is often obscured by superficial and systemic hemodynamic artifacts.⁴ Diffuse optical tomography addresses the limitations of NIRS through a variety of methods. DOT of infant brain function during passive motor activity has been demonstrated using a time-domain DOT system.³⁶ This work established the feasibility of sectioned imaging with DOT of brain activity in infants. However, this method required an acquisition time of up to 2 h per infant for obtaining enough measurements to perform a tomographic reconstruction (generally, the speed of time-domain DOT systems is relatively slow compared with continuous wave illumination systems). Alternatively, HD-DOT systems can provide improved image quality but with the

advantage of ~ 10 Hz full-frame imaging rates. The faster frame-rate enables imaging of single activations within 10 s of stimulus onset when signal to noise ratios are optimal.⁵

With previous studies having established HD-DOT in adults for visual⁶ and motor stimulations,¹¹ the current results indicate that HD-DOT can also improve imaging quality in infants. The DOT responses to the visual stimulus exhibit a bilateral pattern in the majority of the subjects. The bilateral spatiotemporal maps show that the responses are localized to the occipital cortex and are specific to the visual stimulus. These patterns have been observed previously in BOLD-fMRI studies involving young infants^{37,38} and is thought to be an expected cerebral hemodynamic activation response. In contrast, in a topography study in older infants,¹⁵ the images appear to show unilateral responses to visual stimulation. A possible explanation for the absence of bilateral patterns is the lower spatial resolution of the imaging array that did not discriminate left from right cortices as well as contamination from superficial artifacts that might lead to spurious reporting of hemodynamic signals. In addition, our activation maps show increases in both ΔHbO_2 and ΔHbT , and a decreasing trend in ΔHbR during visual stimulation. Although there is some controversy in the literature related to infant neurovascular coupling, our results are similar to previous studies in infants at term, when awake¹⁵ and sleeping/resting,^{13,15} suggesting that, at term, this population has comparable visual responses to healthy adult subjects.

Besides providing improved imaging capability, our results show that the high-density approach can improve data quality in terms of contrast-to-noise ratio improvements of up to $2\times$ (in ΔHbO_2) in the visual responses of seven neonates. Moreover, the DOT temporal responses obtained for each hemodynamic contrast show smoother traces (denoted by smaller variance across stimulus blocks) than the single channel measurements and a stronger resemblance to the expected temporal responses obtained in visual regions in adults and school aged children with fMRI-BOLD.³⁹ The increases in ΔHbO_2 and ΔHbT with respect to baseline are statistically significant consistently across the seven subjects with sufficiently low noise levels. In contrast, only two of the infants showed a statistically significant decrease in ΔHbR . The ΔHbR results might be attributed to either lower signal-to-noise ratio for ΔHbR or to greater variability in the ΔHbR response compared to the ΔHbT and ΔHbO_2 responses.

Visual evoked responses presented a “late overshoot” at the end of the stimulus block in several subjects. This effect is not uncommon in block design studies. A possible explanation is that the inter-stimulus periods were not long enough to allow for the hemodynamic response to completely return to baseline before the next stimulus presentation. Extending the length of the resting period could diminish this effect at the expense of prolonging the overall length of the scanning session. In addition, recent studies⁴⁰ have shown that attention-related oscillating neural signals, phased-locked with the attended stimulus, can be entrained and added to evoked responses. Using experimental paradigms that allow variable inter-block intervals, such as event-related designs, could potentially help to reduce this effect. Nevertheless, it is worth to note that this effect is not present in the group-averaged maps. Further studies on this topic would require larger number of subjects.

While HD-DOT caps enable image reconstructions with improved functional localization, the design and implementation of high-density arrays for newborn infants involves

challenges related to ergonomics of the imaging cap and bulkiness of the fiber bundles. These preliminary results demonstrate the feasibility of using this device to detect brain activity in term-born infants in the nursery during their first days of life. Despite the high channel count of our current system (allowing for 106 measurements for first- and second-nearest neighbor distances), we decided to keep high-density spatial sampling (1 cm) in order to obtain good lateral resolution at the expense of a broader field of view. Future implementations will consider the expansion of the imaging cap to other brain regions (such as frontal, parietal and temporal lobes) that will allow simultaneous evaluation of different functional processes.

In this paper, we used a simplified head model that has demonstrated good performance in visual activation studies in adults.^{6,7} Previous work had shown that anatomical head models derived from high-resolution imaging modalities such as MRI improve imaging and anatomical registration of brain activations in adults⁴¹ and neonates.⁴² Thus possible extensions of this work would consider more realistic head models derived from MRI-based atlases that capture the average geometry and tissue properties of the neonatal head anatomy.

We chose to show feasibility of HD-DOT in infants using visual brain activity since the occipital region has been extensively studied in adults and children. The visual pathway is an early and well-developed sensory area in term-born infants that does not involve active or passive movement of the subject under study (e.g., motor-evoked responses); therefore it is an attractive region for evaluation of functional responses in newborn infants. Yet, there are limitations to visual protocols, mostly related to controlling the level of attention to the stimuli. The variation in the visual cortical activation patterns (e.g., prolonged or asymmetrical activation patterns) seen from several infants in the study may be due to the inherent difficulty in standardizing visual stimulus exposure in infants. Previous studies conducted in awake older infants have used video recordings of the infant’s gaze direction in order to identify data blocks in which the infant did not attend to the visual stimuli.¹⁵ However, in the case of evaluating newborns in the well-infant nursery, it is not possible to implement this strategy since infants often keep their eyes closed during a restful state throughout the scanning session. An alternative way to test the infant’s level of attention/consciousness may be to incorporate a control trial that involves another type of stimulus (e.g., auditory stimulus), which is not expected to activate the occipital cortex.

In conclusion, we have demonstrated the feasibility of performing bedside imaging of evoked responses in neonates in a clinical setting. A parallel study demonstrated that resting-state functional connectivity maps of hospitalized infants can be acquired using the same high-density array.⁸ The combination of both sets of data can significantly improve the robustness and sensitivity of the assessments of the functional architecture and functional connectivity of the infant brain at the bedside. Since the scanning time required for the implementation of each study is approximately 10 min, it is possible to integrate both methodologies into a single protocol for routine clinical use. In this way, HD-DOT has the potential to fulfill the clinical need to provide bedside monitoring and early detection of functional brain deficits in the neonatal population.

Acknowledgments

This work was supported in part by NIH Grants R01-EB009233 (J.P.C.), R21-EB007924 (J.P.C.), T90-DA022871 (Imaging

Science Fellowship, B.R.W.), UL1RR0024992 & UL1TR000448/KL2TR000450 (post-doctoral training and career development grants, S.M.L.), Fulbright Science and Technology Ph.D. Award (S.L.F.), J.P.C. and Washington University have financial interests in Cephalogics LLC based on a license of related optical imaging technology by the University to Cephalogics LLC.

References

1. A. A. Fanaroff, M. Hack, and M. C. Walsh, "The NICHD neonatal research network: changes in practice and outcomes during the first 15 years," *Semin. Perinatol.* **27**(4), 281–287 (2003).
2. C. D. Smyser et al., "Longitudinal analysis of neural network development in preterm infants," *Cereb. Cortex* **20**(12), 2852–2862 (2010).
3. E. Damaraju et al., "Resting-state functional connectivity differences in premature children," *Front. Syst. Neurosci.* **4**(23), 1–13 (2010).
4. B. R. White and J. P. Culver, "A quantitative evaluation of high-density diffuse optical tomography: in vivo resolution and mapping performance," *J. Biomed. Opt.* **15**(2), 026006 (2010).
5. B. R. White and J. P. Culver, "Phase-encoded retinotopy as an evaluation of diffuse optical neuroimaging," *Neuroimage* **49**(1), 568–577 (2010).
6. B. W. Zeff et al., "Retinotopic mapping of adult human visual cortex with high-density diffuse optical tomography," *PNAS* **104**(29), 12169–12174 (2007).
7. B. R. White et al., "Resting-state functional connectivity in the human brain revealed with diffuse optical tomography," *Neuroimage* **47**(1), 148–156 (2009).
8. B. R. White et al., "Bedside optical imaging of occipital resting-state functional connectivity in neonates," *Neuroimage* **59**(3), 2529–2538 (2012).
9. M. D. Fox and M. E. Raichle, "Spontaneous fluctuations in brain activity observed with functional magnetic resonance imaging," *Nat. Rev. Neurosci.* **8**(9), 700–711 (2007).
10. F. T. Sun, L. M. Miller, and M. D'Esposito, "Measuring interregional functional connectivity using coherence and partial coherence analyses of fMRI data," *Neuroimage* **21**(2), 647–658 (2004).
11. S. P. Koch et al., "High-resolution optical functional mapping of the human somatosensory cortex," *Front. Neuroenerget.* **2**(12), 1–8 (2010).
12. D. K. Joseph et al., "Diffuse optical tomography system to image brain activation with improved spatial resolution and validation with functional magnetic resonance imaging," *Appl. Opt.* **45**(31), 8142–8151 (2006).
13. T. Karen et al., "Hemodynamic response to visual stimulation in newborn infants using functional near-infrared spectroscopy," *Hum. Brain Mapp.* **29**(4), 453–460 (2008).
14. J. H. Meek et al., "Regional hemodynamic responses to visual stimulation in awake infants," *Pediatr. Res.* **43**(6), 840–843 (1998).
15. G. Taga et al., "Brain imaging in awake infants by near-infrared optical topography," *Proc. Natl. Acad. Sci. U. S. A.* **100**(19), 10722–10727 (2003).
16. N. M. Gregg et al., "Brain specificity of diffuse optical imaging: improvements from superficial signal regression and tomography," *Front. Neuroenerget.* **2**(14), 1–8 (2010).
17. R. B. Saager, N. L. Telleri, and A. J. Berger, "Two-detector corrected near infrared spectroscopy (C-NIRS) detects hemodynamic activation responses more robustly than single-detector NIRS," *Neuroimage* **55**(4), 1679–1685 (2011).
18. A. Y. Bluestone et al., "Three-dimensional optical tomography of hemodynamics in the human head," *Opt. Express* **9**(6), 272–286 (2001).
19. D. A. Boas et al., "Improving the diffuse optical imaging spatial resolution of the cerebral hemodynamic response to brain activation in humans," *Opt. Lett.* **29**(13), 1506–1508 (2004).
20. S. M. Liao et al., "Neonatal hemodynamic response to visual cortex activity: a high-density NIRS study," *J. Biomed. Opt.* **15**(2), 026010 (2010).
21. M. L. Seghier et al., "Visual recovery after perinatal stroke evidenced by functional and diffusion MRI: case report," *BMC Neurol.* **5**(17), 1–8 (2005).
22. A. Duncan et al., "Measurement of cranial optical path length as a function of age using phase resolved near-infrared spectroscopy," *Pediatr. Res.* **39**(5), 889–894 (1996).
23. S. Wray et al., "Characterization of the near infrared absorption spectra of cytochrome aa3 and haemoglobin for the non-invasive monitoring of cerebral oxygenation," *Biochim. Biophys. Acta* **933**(1), 184–192 (1988).
24. R. Saager and A. Berger, "Measurement of layer-like hemodynamic trends in scalp and cortex: implications for physiological baseline suppression in functional near-infrared spectroscopy," *J. Biomed. Opt.* **13**(3), 034017 (2008).
25. H. Dehghani et al., "Three-dimensional optical tomography: resolution in small-object imaging," *Appl. Opt.* **42**(16), 3117–3128 (2003).
26. G. Strangman, M. A. Franceschini, and D. A. Boas, "Factors affecting the accuracy of near-infrared spectroscopy concentration calculations for focal changes in oxygenation parameters," *Neuroimage* **18**(4), 865–879 (2003).
27. Y. Fukui, Y. Ajichi, and E. Okada, "Monte Carlo prediction of near-infrared light propagation in realistic adult and neonatal head models," *Appl. Opt.* **42**(16), 2881–2887 (2003).
28. M. A. Franceschini et al., "Assessment of infant brain development with frequency-domain near-infrared spectroscopy," *Pediatr. Res.* **61**(5 Pt. 1), 546–551 (2007).
29. A. Gibson et al., "Optical tomography of a realistic neonatal head phantom," *Appl. Opt.* **42**(16), 3109–3116 (2003).
30. D. A. Boas et al., "The accuracy of near infrared spectroscopy and imaging during focal changes in cerebral hemodynamics," *Neuroimage* **13**(1), 76–90 (2001).
31. H. Watanabe et al., "Functional activation in diverse regions of the developing brain of human infants," *Neuroimage* **43**(2), 346–357 (2008).
32. J. Gervain et al., "The neonate brain detects speech structure," *Proc. Natl. Acad. Sci. U. S. A.* **105**(37), 14222–14227 (2008).
33. H. Sato et al., "Cerebral hemodynamics in newborn infants exposed to speech sounds: a whole-head optical topography study," *Hum. Brain Mapp.* (2011), [Epub ahead of print].
34. Y. Minagawa-Kawai et al., "Optical brain imaging reveals general auditory and language-specific processing in early infant development," *Cereb. Cortex* **21**(2), 254–261 (2011).
35. M. Kobayashi et al., "Do infants represent the face in a viewpoint-invariant manner? Neural adaptation study as measured by near-infrared spectroscopy," *Front. Hum. Neurosci.* **5**(153), 1–12 (2011).
36. A. P. Gibson et al., "Three-dimensional whole-head optical tomography of passive motor evoked responses in the neonate," *Neuroimage* **30**(2), 521–528 (2006).
37. E. Martin et al., "Visual processing in infants and children studied using functional MRI," *Pediatr. Res.* **46**(2), 135–140 (1999).
38. H. Yamada et al., "A milestone for normal development of the infantile brain detected by functional MRI," *Neurology* **55**(2), 218–223 (2000).
39. H. C. Kang et al., "Comparison of functional activation foci in children and adults using a common stereotactic space," *Neuroimage* **19**(1), 16–28 (2003).
40. P. Lakatos et al., "Entrainment of neuronal oscillations as a mechanism of attentional selection," *Science* **320**(5872), 110–113 (2008).
41. D. A. Boas and A. M. Dale, "Simulation study of magnetic resonance imaging-guided cortically constrained diffuse optical tomography of human brain function," *Appl. Opt.* **44**(10), 1957–1968 (2005).
42. J. Heiskala et al., "Probabilistic atlas can improve reconstruction from optical imaging of the neonatal brain," *Opt. Express* **17**(17), 14977–14992 (2009).